J Mater Sci (2010) 45:2640–2648
DOI 10.1007/s10853-010-4242-9

Synthesis of nano-MoS_2/TiO_2 composite and its catalytic degradation effect on methyl orange

Kun Hong Hu · Xian Guo Hu · Yu Fu Xu · Jia Dong Sun

Received: 13 August 2009 / Accepted: 15 January 2010 / Published online: 27 January 2010

Abstract A nano-MoS_2/TiO_2 composite was synthesized in H_2 atmosphere by calcining a MoS_3/TiO_2 precursor, which was obtained via a quick deposition of MoS_3 on anatase nano-TiO_2 under a strong acidic condition. The obtained nano-MoS_2/TiO_2 composite was characterized by X-ray diffraction spectroscopy, Brunauer–Emmett–Teller (BET) surface area, scanning electron microscopy, high-resolution transmission electron microscopy, energy-dispersive spectrometry, ultraviolet–visible spectroscopy, and Fourier transform infrared spectroscopy. The results show that the composite had a high BET surface area because of its small size and irregularly layered structure. MoS_2 in the composite was composed of typical layered structures with thicknesses of 2–8 nm and lengths of 10–40 nm. The composite contained a wide and intensive absorption at 400–700 nm, which is in the visible light region, and presented a positive catalytic effect on removing methyl orange from the aqueous solution. The catalytic activity of the composite was influenced by the initial concentration of methyl orange, the amount of the catalyst, the pH value, and the degradation temperature. In addition, the composite catalyst could be regenerated and repeatedly used via filtration three times. The deactivating catalyst could be reactivated after catalytic reaction by heating at 450 °C for 30 min in H_2.

K. H. Hu (✉) · X. G. Hu · Y. F. Xu
Department of Environmental Protection and Monitoring, Hefei University of Technology, 230009 Hefei, China
e-mail: hukunhong@163.com; hukunhong@gmail.com

K. H. Hu · J. D. Sun
Department of Chemical and Materials Engineering, Hefei University, 230022 Hefei, China

Introduction

Molybdenum disulfide (MoS_2) has a typical layered structure with strong interlayer covalent bonds separated by a weak van der Waals gap. The van der Waals gap is generally regarded as an important reason for its catalysis, intercalation, lubrication, anisotropy, chemically inertness, photocorrosion resistance, and specific optical properties. Taking its catalytic properties into consideration, MoS_2 has been vastly used for the removal of S and N from crude oil [1–3]. The importance of MoS_2 as a catalyst lies not only in its relatively high activity but also in its resistance to sulfur poisoning [4]. The nature of the active sites in MoS_2-based catalysts is the main concern of researches. For example, a cluster approach of active sites in MoS_2 catalysts using density functional theory (DFT) calculations was reported [5]. In addition, the "rim-edge" site model was also proposed [6]. With the development in intercalation technology, other MoS_2-based catalysts have also been synthesized [7, 8].

Nanosized MoS_2 has better properties than bulk MoS_2. Thus, it attracts considerable attention. At present, some chemical routes to synthesize nanosized MoS_2 particles have been reported, such as solvothermal [9, 10], hydrothermal [11, 12], inverse micelle method [13], surfactant-assisted synthesis [14], gas synthesis [15], electrochemical methods [16], and decomposition of precursors [17, 18]. Preparing noncrystalline MoS_3 is the key to synthesizing nano-MoS_2. In previous articles [19, 20], a quick homogenous precipitation method was designed to prepare MoS_3 precursor, in various shapes, from sodium molybdate and sulfides. Calcining the precursor at 780 °C could conveniently produce spherical- or slice-like nano-MoS_2 under H_2.

TiO_2 has an excellent photocatalytic activity for use in the removal of unwanted organic chemicals from an aqueous solution. However, the absorption edge of TiO_2

falls in the UV region, which involves only ~3% of the sunlight spectrum. Fortunately, the activity of TiO_2 can be improved by using nanosized TiO_2, mixing active additives to TiO_2, or performing advanced oxidation treatment [21–26]. Alternatively, to deal with such a problem, the photocatalytic capability of nano-MoS_2 was also investigated as a possible solution [13, 27].

The electronic states of the conduction and valence bands in layered bulk MoS_2 are both derived primarily from Mo 4d orbitals. Photoexcitation of electrons, therefore, should not significantly weaken Mo–S bonds, which is responsible for the remarkable photostability of bulk MoS_2 during photoelectrochemical oxidation of water [28, 29]. When the size of MoS_2 is reduced to the nanoscale, such as in films and nanoclusters, Mo edge-site atoms are not protected by the inert basal planes of MoS_2. As a result, the band gap of nanoscale MoS_2 becomes small enough to allow most of the solar spectrum to be harvested. Meanwhile, nano-MoS_2 is relatively unstable in water, leading to the dissolution of the lattice via oxidation of sulfur to sulfate ions. However, this process is quite slow in a covalent material such as this, compared to ionic semiconductor electrodes such as CdS [30]. Thus, it is still possible for nano-MoS_2 to be employed for water treatment.

Based on these facts, nano-MoS_2 reveals a significant advantage over TiO_2, i.e., the band gap of nano-MoS_2 is small enough to allow most of solar light to be absorbed. A possible effective approach to utilizing the photocatalytic function of nano-MoS_2 is to synthesize MoS_2 nanocluster-sensitized TiO_2 [31]. The MoS_2/TiO_2 composite shows potential applications in removing organic chemicals, such as methylene blue, 4-chlorophenol [31], and phenol [30, 32, 33], from wastewater. Moreover, the composite also has good catalytic hydrogenation activities [34] and is a proper hydrodesulfurization catalyst.

Previously, the catalytic activity of MoS_2 nanoclusters obtained by an inverse micelle technique was investigated by Thurston and Wilcoxon [30] and Wilcoxon et al. [32]. In the method, MoS_2 nanoclusters were formed by combining Mo (IV) halide and sulfide in inverse micelle solutions. A major drawback for this method is that Mo (IV) halides are not stable compounds. Thus, a modified hydrothermal method was reported to address this problem [33]. In the modified method, nano-MoS_2 was synthesized in a sealed autoclave under continuous stirring for 5 h at 180 °C. The MoS_2/TiO_2 catalysts were then prepared by dispersing nano-MoS_2 and TiO_2 in ethanol using a high-speed homogenizer. Though the hydrothermal method was an effective approach to synthesizing MoS_2 nanoparticles, it was not very convenient because of the need for high-pressure equipment. Moreover, this method did not provide a direct method for obtaining nano-MoS_2/TiO_2 composites. To overcome these disadvantages, the MoS_3/TiO_2 composite was synthesized by a quick deposition of MoS_3 on acid-activated TiO_2. The nano-MoS_2/TiO_2 composite was then prepared by calcining the obtained MoS_3/TiO_2 composite. The resultant nano-MoS_2/TiO_2 composite from this particular route showed a high catalytic activity for the removal of methyl orange from an aqueous solution.

Experiment

Materials

The anatase nano-TiO_2 photocatalyst was provided by Zixilai Company, China (the detailed information can be found on http://www.zixilai.com/en/product_display.asp?keyno=1). HCl, $Na_2S{\cdot}9H_2O$, $Na_2MoO_4{\cdot}2H_2O$, and other reagents were of analytical grade.

Synthesis of nano-MoS_2/TiO_2 composite

A typical preparation process is described as follows: 0.6 g $Na_2MoO_4{\cdot}2H_2O$ and 3.4 g $Na_2S{\cdot}9H_2O$ were dissolved in 100-mL de-ionized water. Then, 10-mL alcohol was added into the reaction system. Anatase nano-TiO_2 was dispersed in the obtained solution, and 4.0 mL 12-M HCl was dumped into the reaction system. The resultant precipitation was washed by de-ionized water and dried at 120 °C. The as-synthesized precursor was calcined in a tube furnace at 450 °C for 30 min under a flow of highly pure hydrogen (99.999%). The desired nano-MoS_2/TiO_2 samples were obtained. Nano-MoS_2 sample without TiO_2 was also prepared by a similar method.

Characterization

Powder X-ray diffraction (XRD) was performed on a Rigaku model D/Max-γB diffractometer with Cu K_α radiation. Micrographs were obtained using a JEOL model 2010 high-resolution transmission electron microscopy (HRTEM) with energy-dispersive spectrometry (EDS) and an FEI model Sirion 200 field emission scanning electron microscope (SEM). The Brunauer–Emmett–Teller (BET) surface area was determined using a Micromeritics model ASAP 2020M+C physical and chemical adsorption analyzer. Ultraviolet–visible (UV–vis) light spectral analysis was done on a Shimazu model UV-2550 UV–vis spectrometer. Fourier transform infrared (FTIR) spectra was recorded using a Shimazu model FTIR-8400S IR spectrometer.

Catalytic experiments

The photocatalytic activities of the obtained composite catalysts were evaluated according to the decoloration rate

(%) of the methyl orange solution in a quartz glass reactor. Two main light sources were selected as environmental lights, including outdoor direct sunlight and indoor weak sunlight, with a 30-W daylight lamp for illumination. The UV light was weak enough to be neglected, and only the visible light was considered in the indoor environment. To avoid the influence from the instability of the used light, the same serial experiments were done as simultaneously as possible. A typical catalytic experiment is described as follows:

First, 0.1-g nano-MoS_2/TiO_2 was added into a 150 mL 20-mg/L methyl orange solution, and the obtained suspension was placed in a darkroom and stirred for 10 min to complete the adsorption balance. Then, the catalytic reaction continued for 120 min under the indoor visible light. About 2 mL of reaction suspension was sucked after every 30 min using an injector. Then, it was clarified by 3,000 r/min centrifugation for 5 min. The absorbance (A) of the clarified solution was measured on a 721 spectrophotometer (Shanghai Precision & Scientific Instrument Company, China). The decoloration rate (%) was accounted for according to the formula: decoloration rate (%) = $(A_0 - A)/A_0$. After the catalytic reaction, the suspension was filtered. One part of the filtration residue was used for IR characterization and the other for investigating the regeneration of catalyst.

Results and discussion

Synthesis and characterization of nano-MoS_2/TiO_2 composite

The composite [MoS_2/TiO_2 (wt/wt) = 6:5, calculated according to the weight change in the obtained precipitation] was fully characterized. The XRD patterns of the nano-TiO_2 and nano-MoS_2/TiO_2 composites at 450 °C are shown in Fig. 1. The nano-TiO_2 XRD pattern in Fig. 1a is consistent with that in PDF#89-4921 belonging to the anatase TiO_2. All diffraction peaks of anatase nano-TiO_2 were still present in the XRD pattern of the nano-MoS_2/TiO_2 composite (Fig. 1b), indicating that the anatase nano-TiO_2 was not destroyed during the synthesis process. Moreover, in Fig. 1b, it can be noted that the XRD pattern of nano-MoS_2 included four main diffraction peaks, i.e., (002), (100), (103), and (110), which is consistent with that reported in a previous study [20]. All the XRD peaks in Fig. 1b can be indexed to anatase TiO_2 and nano-MoS_2, indicating that possible new phases, such as TiS_2 and MoO_2, were not formed. The findings confirm that the nano-MoS_2/TiO_2 composite was successfully prepared.

An SEM image of the prepared nano-MoS_2/TiO_2 composite is shown in Fig. 2. The composite formed

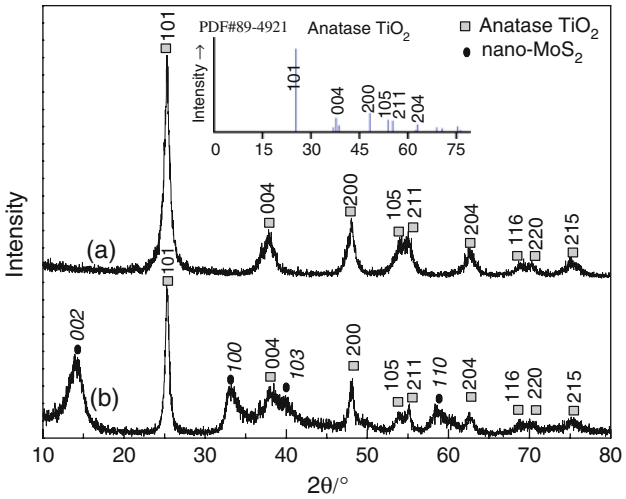

Fig. 1 XRD patterns of samples (*a*) TiO_2 and (*b*) nano-MoS_2/TiO_2 composites

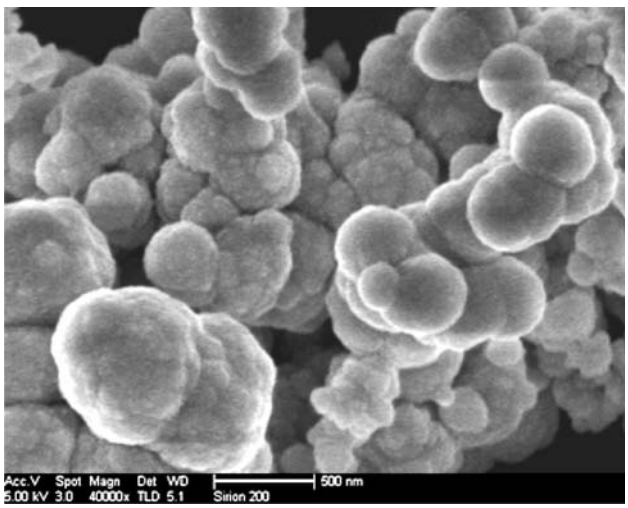

Fig. 2 SEM image of the prepared nano-MoS_2/TiO_2 composite

homogenous clusters with pores. The composite clusters had sizes of 100–600 nm and were composed of small nanoparticles.

The EDS analysis of the prepared nano-MoS_2/TiO_2 composite is presented in Fig. 3. It can be seen that the composite mainly contained Mo, S, Ti, and O, and the Cu, C, and Cr peaks were ascribed to the copper net and carbon film, which were used in the EDS characterization.

HRTEM images are illustrated in Figs. 4a–d. As shown in the two images of Figs. 4a and b (a typical inner region), nano-MoS_2 particles were homogenously distributed among TiO_2 particles and composed of typical layered structures with an average length of about 15 nm (10–20 nm) and an average thickness of about 5 nm (2–8 nm). However, the layered structure on the surface of

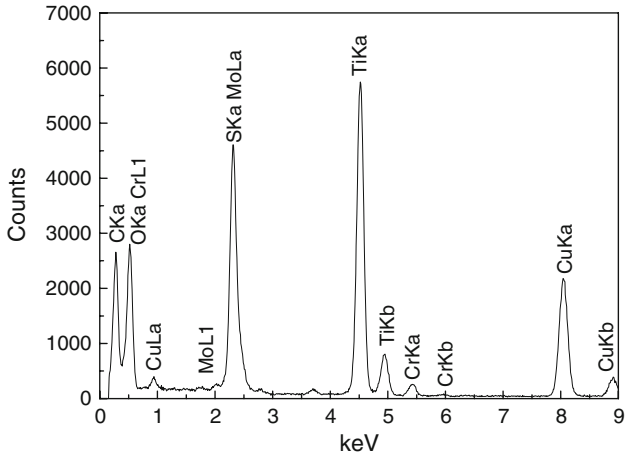

Fig. 3 EDS analysis of the prepared nano-MoS_2/TiO_2 composite

the composite showed a different size from the interior one according to Fig. 4c and d. The average length of the nano-MoS_2 particles on the surface was increased by 10–20 nm compared with the ones in the interior. The increase in size was ascribed to the weak steric hindrance on the surface.

It is well known that nano-MoS_2 can be prepared according to the following reactions [20]:

$$4S^{2-} + MoO_4^{2-} + 10H^+ \rightarrow MoS_3 \downarrow + H_2S \uparrow + 4H_2O,$$

$$MoS_3 + H_2 \xrightarrow{780\,^\circ C} \text{nano-}MoS_2 + H_2S.$$

The first reaction mentioned above can be mixed with TiO_2 to produce the nano-MoS_3/TiO_2 composite.

$$S^{2-} + MoO_4^{2-} + 10H^+ + TiO_2 \rightarrow MoS_3/TiO_2 \downarrow + H_2S \uparrow + 4H_2O.$$

Though nano-TiO_2 is not soluble in the acid solution, there still existed a balance on the inner and external surfaces of TiO_2 when high-concentration strong acid was used.

$$TiO_2 + 4H^+ \rightleftharpoons Ti^{4+} + 2H_2O.$$

Such reaction led to the activation of the TiO_2 surface and provided nucleation sites on the surface, where MoS_3 can easily deposit to form a homogenous composite.

High temperatures and long calcining time can increase the crystalline degree of MoS_2. However, they can also

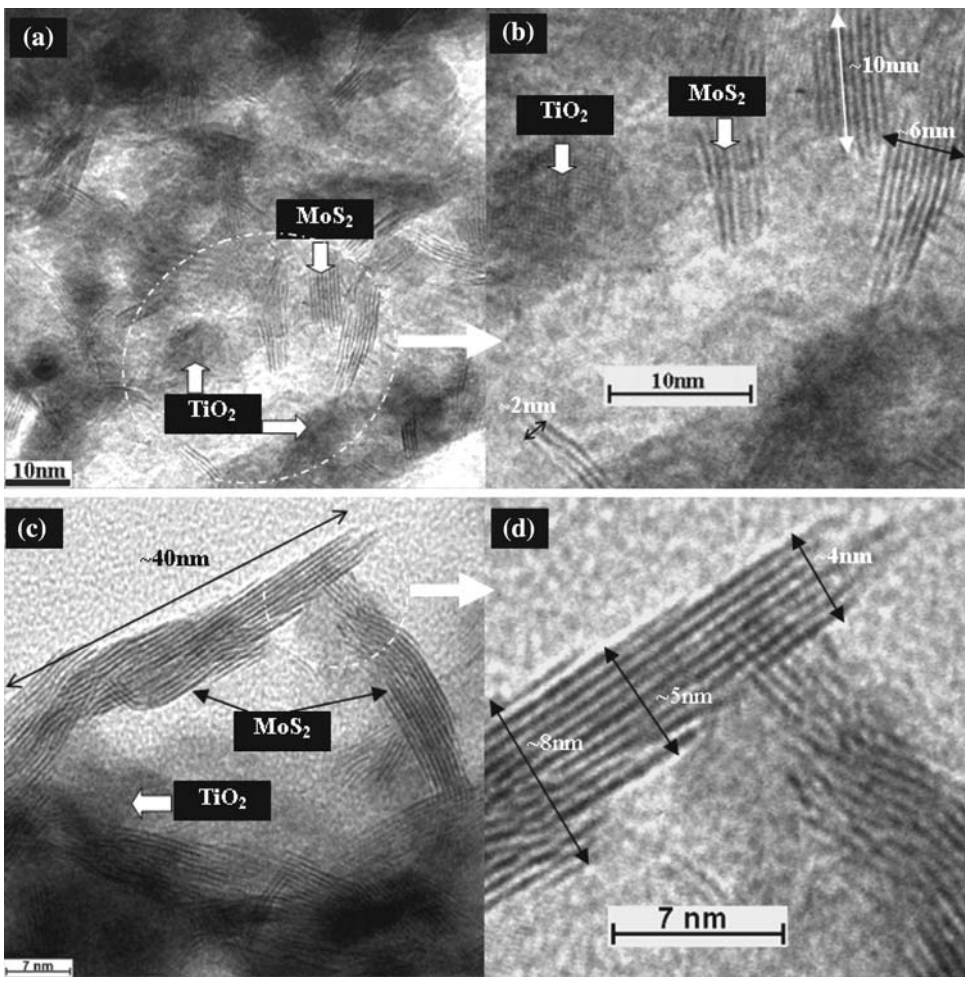

Fig. 4 HRTEM micrographs of the prepared nano-MoS_2/TiO_2 composite: **a** typical inner region, **b** magnified image of (**a**), **c** typical region of the surface, and **d** magnified image of (**c**)

lead to the crystal transformation of anatase TiO_2 into rutile TiO_2. Moreover, high temperatures and long-treatment periods also possibly inspire the reaction of TiO_2 and H_2S, leading to TiS_2. To avoid these disadvantages, a relatively low calcining temperature of 450 °C and a short treatment time of 30 min were applied in this work.

$$MoS_3/TiO_2 + H_2 \xrightarrow{450\,^{\circ}C/30\,min} nano - MoS_2/TiO_2 + H_2S.$$

UV–vis light spectra of the prepared nano-MoS_2/TiO_2 composite and nano-MoS_2 are shown in Fig. 5. The UV–vis spectrum of the nano-MoS_2/TiO_2 composite reveals five peaks labeled as (1)–(5) (cf. Fig. 5a). Peaks (1) and (3)–(5) were also found in the UV–vis spectrum in Fig. 5b, belonging to the nano-MoS_2 prepared via a similar method but without nano-TiO_2. It was confirmed that both nano-MoS_2 and nano-MoS_2/TiO_2 composite had observable absorbances in the visible light region. Peak (2) in Fig. 5a can be ascribed to the absorption of nano-TiO_2 in the UV region, which is consistent with the result reported in a previous article [21]. The other interesting observation is that the combination of nano-MoS_2 and nano-TiO_2 weakened the absorption of nano-MoS_2 in the UV region [peak (1) in Fig. 5a].

Thurston and Wilcoxon [30] reported that the absorption peak of MoS_2 (d = 8–10 nm) was at ~700 nm, while that of MoS_2 (d = 4.5 nm) was at ~470 nm in the visible light region. The nano-MoS_2/TiO_2 used in this work showed absorption peaks at ~470 and 600–700 nm. The nano-MoS_2 in the composite exhibited varying sizes (including length and thickness) from 2 to 40 nm, which led to the appearance of the two absorption peaks in the visible light region. It was very significant that the two absorption peaks connected to each other and led to a wide absorption in the visible light region. Moreover, it has been found that the bulk MoS_2 has absorption edges at 1040 nm (1.23 eV band gap) [35]. The large blueshifts of nano-MoS_2 result from its strong quantum confinement effect [13, 30, 36, 37]. The quantum effect also increases the band gap of nano-MoS_2, and its redox potentials are accordingly changed. The appropriate alternation in the energy levels of the conduction and valence band edges allow MoS_2 nanoclusters to act as sensitizers for visible light-TiO_2 photocatalysis [31].

Table 1 BET surface areas of samples

Sample	Anatase TiO_2	Nano-MoS_2/TiO_2	Nano-MoS_2
BET surface area (m^2/g)	226.6	91.5	30.8

To investigate the influence of the surface area, BET surface areas were measured and are listed in Table 1. The nano-MoS_2 exhibited a relatively low BET surface area (30.8 m^2/g), and the anatase nano-TiO_2 had the highest BET surface area (226.6 m^2/g). The surface area of the nano-MoS_2/TiO_2 composite increased to 91.4925 m^2/g when nano-MoS_2 was combined with anatase nano-TiO_2.

Catalytic activity of MoS_2/TiO_2 composite

Taking the instability of the indoor and outdoor sunlight into account, the same serial catalytic experiments were done as simultaneously as possible, and the results are shown in Fig. 6. As shown in this figure, the highest catalytic activity appeared in the composite with a weight ratio of 6:5 (MoS_2/TiO_2). Although anatase nano-TiO_2 had the highest BET surface area (226.6 m^2/g), it still showed a very low activity for degrading methyl orange under indoor visible light. This is because its absorption occurs in the UV region. Though nano-MoS_2 had a low BET surface area (30.8 m^2/g), it had an obvious absorption in the visible light region and exhibited a high activity for the degradation of methyl orange. The deposition of nano-MoS_2 on the anatase nano-TiO_2 surface considerably increased the surface area of the composite catalyst to 91.5 m^2/g. The absorbance of nano-MoS_2 in the visible light region was maintained even in the composite form (Fig. 5). Therefore, the nano-MoS_2/TiO_2 composite showed the highest catalytic activity among the three catalysts.

The influence of the light source on the decoloration rate of methyl orange is still present in Fig. 6. As shown in this

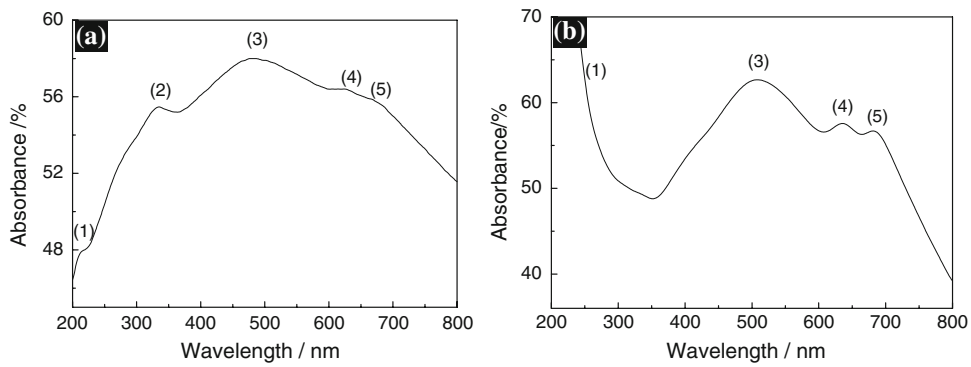

Fig. 5 UV–vis light spectra of the prepared samples. **a** Nano-MoS_2/TiO_2 composite and **b** nano-MoS_2

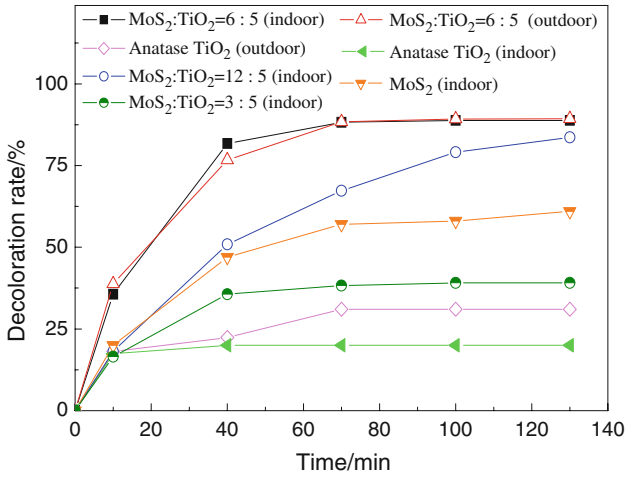

Fig. 6 Influence of catalyst composition on the decoloration rate of methyl orange solution [reaction conditions: 10 °C, 0.1-g catalyst, c_0 (methyl orange) = 20 mg/L, V = 150 mL]

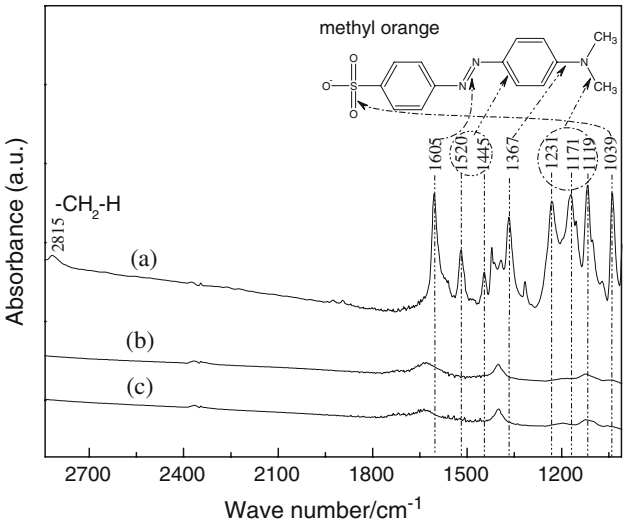

Fig. 7 IR spectra of samples. **a** Pure methyl orange, **b** nano-MoS_2/TiO_2 after catalytic degradation of methyl orange, and **c** nano-MoS_2

figure, anatase nano-TiO_2 had no catalytic activity for degrading methyl orange under indoor visible light, but it showed slight activity under outdoor direct sunlight after 10-min adsorption balance. Because the optical absorption of TiO_2 falls in the UV region, it showed a slight activity under outdoor sunlight, which contains ~3% UV light. However, the prepared nano-MoS_2/TiO_2 composite catalyst represented a very high catalytic activity for the degradation of methyl orange under both indoor visible light and outdoor sunlight. The nano-MoS_2/TiO_2 composite had an obvious absorption in the visible light region according to Fig. 5, leading to its excellent catalytic activity for degrading methyl orange. Because the absorption of the composite is very wide in the visible light region, the light source has almost no considerable influence on the catalytic activity of the composite.

In addition, the decoloration rate in Fig. 6 increased by 1% from 75 min (~88%) to the end of the experiment (~89%). This indicates that 0.1-g catalyst was not enough to degrade methyl orange completely, and thus the decoloration rate increased slowly in the end. This will be discussed in the section concerning the influence of the amount of catalyst.

IR spectroscopy was used to clarify that the high decoloration rate of methyl orange was not caused by its adsorption, and the results are shown in Fig. 7. Pure methyl orange represented a lot of transmittance peaks at 1000–1700 cm^{-1} (cf. Fig. 7a), and the main peaks are marked in this figure. The IR spectrum of the nano-MoS_2/TiO_2 composite after catalytic reaction is shown in Fig. 7b. It is similar to that of pure nano-MoS_2 (Fig. 7c), in which the peaks belonging to methyl orange cannot be found. These peaks belong to the functional groups like –N=N–, benzene ring, and –N–C–. This finding indicates that the adsorbed methyl orange on the surface of the composite catalyst degraded completely. Therefore, the decoloration of the methyl orange solution was induced by the degradation rather than by the adsorption of methyl orange on nano-MoS_2/TiO_2.

The catalytic activity of the nano-MoS_2/TiO_2 catalyst under visible light was attributed to the electron transfer from the conduction band of the quantum-sized nano-MoS_2 to TiO_2. Under visible light, only MoS_2 was activated. The photoexcited electron was then scavenged by the oxygen in the water, finally forming hydroxyl radicals to degrade the organic chemicals [31]. It was difficult to clarify the catalytic mechanisms for MoS_2 and TiO_2 by designing experiments in this article, so instead a speculative mechanism that has been proposed in literature [31, 37] is presented:

$$MoS_2/TiO_2 + hv \rightarrow MoS_2(h^+ + e^-)/TiO_2,$$

$$MoS_2(h^+ + e^-)/TiO_2 \rightarrow MoS_2(h^+)/TiO_2(e^-),$$

$$TiO_2(e^-) + O_2 \rightarrow TiO_2 + O_2^-,$$

$$O_2^- + H_2O \rightarrow HO_2^\bullet + OH^-,$$

$$HO_2^\bullet + H_2O \rightarrow H_2O_2 + OH^\bullet,$$

$$H_2O_2 \rightarrow 2OH^\bullet,$$

$$OH^\bullet + \text{organic compound} \rightarrow CO_2 + H_2O.$$

Because methyl orange contains element S and the reaction product of SO_4^{2-} was detected by adding $BaCl_2$ during the catalytic tests, the reaction of the degradation is summarized as follows:

$$OH^{\bullet} + \text{methyl orange} \rightarrow CO_2 + H_2O + SO_4^{2-}$$

Though the degradation process, with a number of degradation products, is very complex, the degradation mechanism of methyl orange was well studied by Baiocchi et al. [38].

Effect of degradation conditions

The influence of the amount of nano-MoS_2/TiO_2 on the decoloration rate of methyl orange solution is shown in Fig. 8a. Generally, the catalytic capability can be improved with increasing amounts of the catalyst. In this study, the decoloration rate of the methyl orange solution also increased with increasing contents of the catalysts. When the amount of the catalyst was increased to 0.2 g/150 mL methyl orange solution, the decoloration rate within 2 h attained a satisfactory value (95.1%). This implies that the optimal amount of the composite catalyst was about 0.2 g/150 mL methyl orange under the given reaction conditions. However, taking economy and convenience into account, 0.1-g catalyst was used in this study, with which the methyl orange had an ~89% decoloration rate.

The effect of the initial concentration of methyl orange on the decoloration rate is shown in Fig. 8b. The decoloration rates decreased when the initial concentrations increased. The decoloration was satisfactory only when the initial concentrations were about 10–20 mg/L. The higher initial concentrations exceeded the treatment capability of the 0.1-g composite catalyst used.

The degradation curves at different temperatures are shown in Fig. 8c. When 0.1-g catalyst was employed in the 150-mL solution, the decoloration rate at 0–20 °C was relatively high, reaching a peak at 10 °C. However, the decoloration rate became unsatisfactory at 30 °C. When the temperature was increased to 50 °C, a high decoloration rate again occurred. The optimal degradation temperature was about 10 or 50 °C. The low activity of the composite at 30 °C seemed to reduce the application of the catalyst in some regions, particularly at ambient temperature between 20 and 30 °C. However, the shortcoming may be offset by increasing the amount of the catalyst. When the content of the catalyst was increased to 0.2 g/150 mL solution, the methyl orange also exhibited a very high decoloration rate.

The relationship between the degradation temperature and the decoloration rate is very complex. High temperatures can generally increase the reaction rate but decrease the adsorption of methyl orange on the catalyst. The harmony of the two conflicting factors led to excellent catalytic activity at about 10 °C (Fig. 8c). Besides the temperature, other factors, such as thermal effect of the degradation reaction, influence of vapor on the absorbance, and hydrolyzation of methyl orange, also have impacts on the degradation reaction. The thermodynamics and kinetics of the nano-MoS_2/TiO_2 catalyst need to be specially studied.

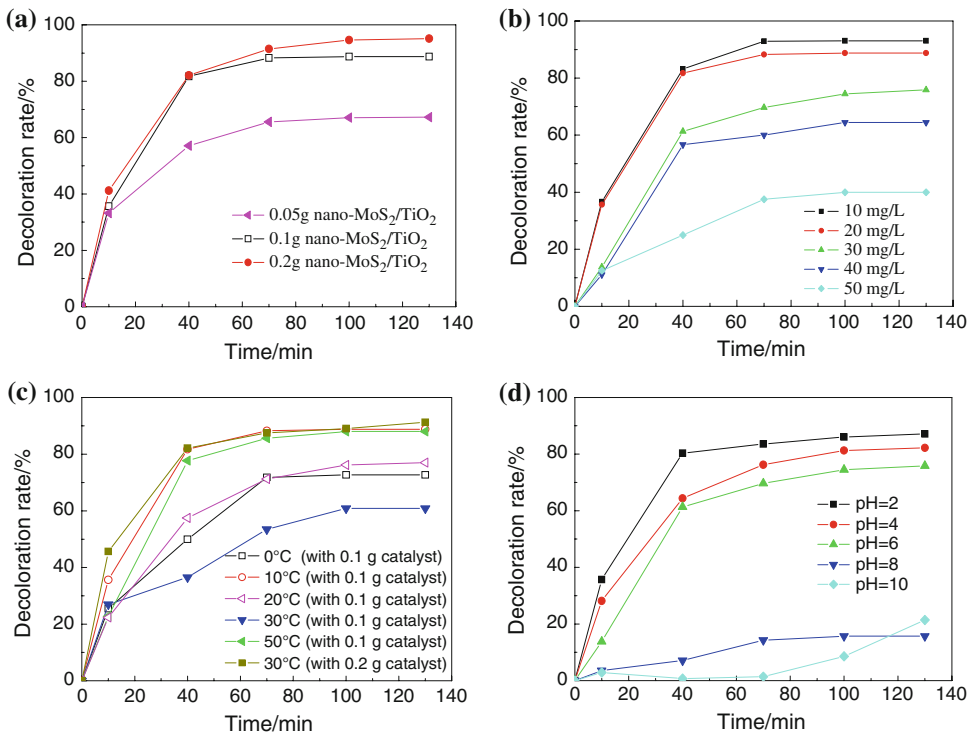

Fig. 8 Effect of conditions on the decoloration rate of methyl orange: **a** nano-MoS_2/TiO_2 amount, **b** initial concentration of methyl orange, **c** degradation temperature, and **d** initial pH value

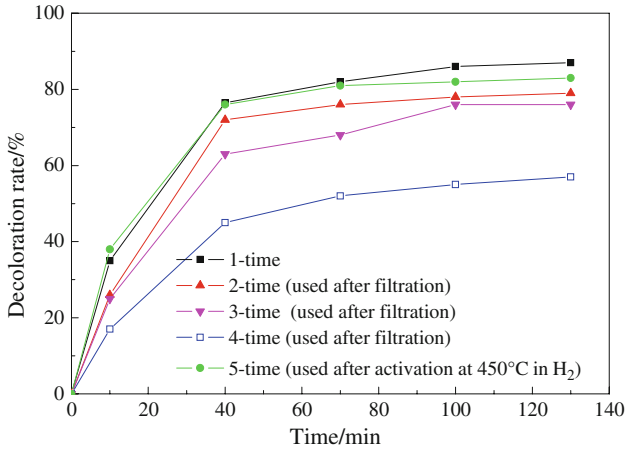

Fig. 9 Influence of the repeated use of the nano-MoS_2/TiO_2 catalyst on the decoloration rate of the methyl orange solution

The influence of the initial pH values on the decoloration rate of methyl orange solution is shown in Fig. 8d. The initial pH value was one of important parameters in the degradation reaction of methyl orange. The acidic condition of the aqueous solution accelerated the degradation of methyl orange. However, methyl orange exhibited a very low decoloration rate under alkaline conditions. It includes two molecular structures, i.e., azo methyl orange under alkaline condition and quinoid methyl orange under acidic condition. The easy degradation of methyl orange under acidic condition indicates that the nano-MoS_2/TiO_2 catalyst had a higher activity for the degradation of the quinoid methyl orange rather than the azo methyl orange.

Regeneration of the nano-MoS_2/TiO_2 catalyst

The influence of the repeated use of the nano-MoS_2/TiO_2 catalyst on the decoloration rate of the methyl orange solution is shown in Fig. 9. The nano-MoS_2/TiO_2 catalysts regenerated via filtration held high catalytic activities after three repeated uses. The activity of the four-time regenerated catalyst almost became weak. However, the catalyst could be reactivated via heating at 450 °C in H_2 atmosphere (cf. Fig. 9).

Conclusion

A novel large-scale preparation of the nano-MoS_2/TiO_2 composite is presented. The obtained nano-MoS_2/TiO_2 composite has a high BET surface area and a wide absorption in the visible light region, which leads to high catalytic activity in methyl orange degradation. The composite catalyst may be regenerated by filtration and reactivated by heating in H_2. The composite is one of the promising photocatalytic materials for the removal of organic chemicals from wastewater, such as organic dyes and phenols. The composite perhaps also has potential applications in the hydrodesulfurization of crude oil and the catalytic oxidation of S^{2-}.

Acknowledgements The financial support from the National Key Technology R&D Program of China (Grant No. 2007BAD34B02), National Natural Science Foundation of China (Grant No. 50905054), Anhui Provincial Natural Science Foundation (Grant No. 070414152), and Anhui Provincial Foundation for Excellent Young Talents in University (Grant No. 2010SQRL160) is highly appreciated.

References

1. Valyon J, Hall WK (1983) J Catal 84:216
2. Richardson JT (1988) J Catal 112:313
3. Millman WS, Segawa K, Smrz D, Hall WK (1986) Polyhedron 5:169
4. Moore SE, Lunsford JH (1982) J Catal 77:297
5. Faye P, Payen E, Bougeard D (1999) J Mol Model 5:63
6. Daage M, Chianelli RR (1994) J Catal 149:414
7. Miremadi BK, Morrison SR (1987) J Catal 103:334
8. Miremadi BK, Morrison SR (1988) J Catal 112:418
9. Peng YY, Meng ZY, Zhong C, Lu J, Yang ZP, Qian YT (2002) Mater Chem Phys 73:327
10. Zhan JH, Zhang ZD, Qian XF, Wang C, Xie Y, Qian YT (1998) J Solid State Chem 141:270
11. Li WJ, Shi EW, Ko JM, Chen ZZ, Ogino H, Fukuda T (2003) J Cryst Growth 250:418
12. Li XL, Li YD (2004) J Phys Chem B 108:13893
13. Wilcoxon JP, Newcomer PP, Samara GA (1997) J Appl Phys 81:7934
14. Afanasiev P, Xia GF, Berhault G, Jouguet B (1999) Chem Mater 11:3216
15. Feldman Y, Wasserman E, Srolovitz DJ, Tenne R (1995) Science 267:222
16. Zach MP, Inazu K, Ng KH, Hemmingr JC, Penner RM (2002) Chem Mater 14:3206
17. Nath M, Govindaraj A, Rao CNR (2001) Adv Mater 13:283
18. Zou TZ, Tu JP, Huang HD, Lai DM, Zhang LL, He DN (2006) Adv Eng Mater 8:289
19. Hu KH, Wang YR, Hu XG, Wo HZ (2007) Mater Sci Technol 23:242
20. Hu KH, Hu XG (2009) Mater Sci Technol 25:407
21. Chatterjee D, Mahata A (2002) J Photochem Photobiol A 153:199
22. Min SX, Wang F, Han YQ (2007) J Mater Sci 42:9966. doi: 10.1007/s10853-007-2074-z
23. Randeniya LK, Murphy AB, Plumb IC (2008) J Mater Sci 43:1389. doi:10.1007/s10853-007-2309-z
24. Castro AL, Nunes MR, Carvalho AP, Costa FM, Florêncio MH (2008) Solid State Sci 10:602
25. Reddy BM, Reddy GK, Rao KN, Ganesh I, Ferreira JMF (2009) J Mater Sci 44:4874. doi:10.1007/s10853-009-3743-x
26. Jiang BT, Zhang SY, Guo XZ, Jin BK, Tian YP (2009) Appl Surf Sci 255:5975
27. Iliev V, Prahov L, Bilyarska L, Fischer H, Schulz-Ekloff G, Wöhrle D, Petrov L (2000) J Mol Catal A 151:161
28. Tributsch H (1977) Z Naturforsch 32a:972
29. Pelizzetti E, Visca M (1983) In: Gratzel M (ed) Energy resources through photochemistry and catalysis. Academic Press, New York, p 261

30. Thurston TR, Wilcoxon JP (1999) J Phys Chem B 103:11
31. Ho WK, Yu JC, Lin J, Yu JG, Li PS (2004) Langmuir 20:5865
32. Wilcoxon JP, Thurston TR, Martin JE (1999) Nanostruct Mater 12:993
33. Pourabbas B, Jamshidi B (2008) Chem Eng J 138:55
34. Shimada H (2003) Catal Today 86:17
35. Kam KK, Parkinson BA (1982) J Phys Chem 86:463
36. Huang JM, Laitinen RA, Kelley DF (2000) Phys Rev B 62:10995
37. Wilcoxon JP (2000) J Phys Chem B 104:7334
38. Baiocchi C, Brussino MC, Pramauro E, Prevot AB, Palmisano L, Marcì G (2002) Int J Mass Spectrom 214:247